

University of Nebraska - Lincoln

DigitalCommons@University of Nebraska - Lincoln

Theses, Dissertations, and Student Research from
Electrical & Computer Engineering

Electrical & Computer Engineering, Department of

5-2017

Smart Feedback Control for Fiber-optics Acoustic Emission Sensor System

Xiangyu Luo

University of Nebraska-Lincoln, shawn-yu@huskers.unl.edu

Follow this and additional works at: <http://digitalcommons.unl.edu/elecengtheses>



Part of the [Electrical and Electronics Commons](#), and the [Electromagnetics and Photonics Commons](#)

Luo, Xiangyu, "Smart Feedback Control for Fiber-optics Acoustic Emission Sensor System" (2017). *Theses, Dissertations, and Student Research from Electrical & Computer Engineering*. 79.

<http://digitalcommons.unl.edu/elecengtheses/79>

This Article is brought to you for free and open access by the Electrical & Computer Engineering, Department of at DigitalCommons@University of Nebraska - Lincoln. It has been accepted for inclusion in Theses, Dissertations, and Student Research from Electrical & Computer Engineering by an authorized administrator of DigitalCommons@University of Nebraska - Lincoln.

SMART FEEDBACK CONTROL FOR FIBER-OPTIC ACOUSTIC EMISSION

SENSOR SYSTEM

by

Xiangyu Luo

A THESIS

Present to the Faculty of

The Graduate College at the University of Nebraska

In Partial Fulfillment of Requirements

For the Degree of Master of Science

Major: Electrical Engineering

Under the Supervision of Professor Ming Han

Lincoln, Nebraska

May 2017

Smart feedback control for fiber-optic acoustic emission sensor system

Xiangyu Luo, M.S.

University of Nebraska, 2017

Advisor: Ming Han

Optical fiber sensors for ultrasonic detection have become a subject of much research in recent years. In this thesis, a fiber-optic acoustic emission (AE) sensor system that is capable of performing AE detection, even when the sensor is experiencing large quasi-static strains, is first described. The system consists of a smart selection of a wavelength notch to which a distributed feedback (DFB) laser is locked for high sensitivity AE signal demodulation. A smart feedback control unit for the DFB laser, which is the focus of this thesis, is designed and investigated. The smart control ensures that the AE signal is monitored without significant disruption even when large external strains are superimposed on the sensor.

Using a chirped fiber-Bragg-grating Fabry–Perot interferometer (CFBG-FPI) sensor head, the performance of the designed feedback controller has been examined. Experiments were conducted on an aluminum plate which in the meantime was subject to a large background strain variation. The large external strain shifted the Bragg wavelength by six spectral notches of the CFBG-FPI and thus led to a total of six locking point “jumps” to accommodate the large strain change while the AE signals were continuously monitored with minute disruption. The designed smart control proved to

work properly for the fiber-optic acoustic emission system. In the end of this thesis, characteristics of wavelength tuning, in terms of wavelength scanning range and delay as a function of tuning frequency, of a narrow linewidth semiconductor has been investigated. This narrow linewidth laser based on quantum well theory has much lower intensity and frequency noise in comparison with the DFB laser used in our previous experiments, and thus will serve as a promising candidate for next generation AE sensor with enhanced performance.

ACKNOWLEDGEMENTS

First, I would like to thank my advisor, Dr. Ming Han, for the opportunity to work on this down to earth project. In addition, the instruction he has provided over the last two years has been indispensable. He has helped me to grow as a critical thinker, a real engineer and provided a path for me to do so.

I would like to thank my thesis review committee, Professor Dennis Alexander and Professor Eva Franke-Schubert, for their time in examining my thesis and participating in its review.

I would like to thank the colleagues in my research group Qi Zhang, Guigen Liu, and Yupeng Zhu advice and assistance. I would furthermore like to thank Qi Zhang for her work helping me with the integration between electronic control devices and theoretical work on optical censoring devices. Thank Yupeng Zhu for fabricate the sensor heads, select power supply, and packaging.

I would sincerely like to show my gratitude to my family, especially my parents, who have been my support over the last seven years. My friends help me overcome the culture shocks, and blend in with the Nebraskan.

This work is supported by the Office of Naval Research under grant number N000141410139 and N000141410456.

CONTENTS

ACKNOWLEDGEMENTS	iv
TABLE OF FIGURE	vii
CHAPTER 1: INTRODUCTION	1
1.1 Background & Motivation	1
1.1.1 Current state of the art of acoustic emission (AE) sensors	1
1.1.2 Advantage of Fiber-optic Sensor	1
1.1.3 Challenge of fiber-optics sensors.....	2
1.2 Chirped fiber-Bragg-grating Proposal.....	3
1.2.1 Solve the Challenge	3
1.2.2 Thesis Structure	4
CHAPTER 2: SMART FEEDBACK CONTROLLER.....	5
2.1 Description of the Sensor System.....	5
2.1.1 Operation Principle of the Sensor Head.....	5
2.1.2 Laser and Laser Controller.....	8
2.1.3 Role of the smart feedback control unit.....	9
2.2 Design of the smart feedback control unit	9
2.2.1 Partial – Integral (P-I) Feedback Controller	10
2.2.2 Smart Feedback Controller	12
2.2.3 Modulation signal design.....	15
2.2.4 Implementation of Modulation Signals	16
2.2.5 Digital to Analog Converter.....	17
2.3 Experiment Demonstration	18

2.3.1 System Setup.....	18
2.3.2 Setting Locking Point	19
2.3.3 Locking	21
2.3.4 Jump Towards Longer wavelength.....	22
2.3.5 Jump to the Shorter Wavelength.....	25
2.4 Instrumentation	26
2.5 Summary	27
CHAPTER 3: CHARACTERIZATION OF NARROW LINEWIDTH LASER.....	29
3.1 Mechanism of Laser Wavelength Modulation.....	29
3.1.1 Measurement of Wavelength Tuning.....	29
3.1.2 Theory of Mach–Zehnder Interferometer(MZI)	30
3.2 Measurement setup	31
3.2.1 Response to Step Current Modulation	31
3.2.2 Sinusoidal Modulation.....	33
3.3 Summary	36
Chapter 4: CONCLUSION.....	38
4.1 Summary	38
4.2 Future Work	39
REFERENCE.....	40

TABLE OF FIGURE

Figure 2.1 Effective cavity length L_{eff} changes with wavelength for identical chirped pair FP cavity	6
Figure 2.2 CFBG spectrum profile for this experiment	7
Figure 2.3 Example of laser intensity-demodulation	8
Figure 2.4 (a) Linewidth of the narrow linewidth laser	9
Figure 2.5: Feedback Controller System Block Diagram	10
Figure 2.6 A Partial Integral System	12
Figure 2.7: Demonstration of seeking new locking point	14
Figure 2.8 Example of a Modulation Signal	15
Figure 2.9: Digital - to - Analog circuits schematics	18
Figure 2.10 Schematic of the experimental setup	19
Figure 2.11 finding locking point using scanning method	20
Figure 2.12 (a)–(f) Reflection spectra of the five spectral notches used for AE detection; corresponding (g)–(l) AE signals	22
Figure 2.13 Control and monitor signals of the smart feedback control unit when the sensor was compressed	24
Figure 2.14 Control and monitor signals of the smart feedback control unit when the sensor was extended	26
Figure 3.1 Fiber Mach–Zehnder interferometer Schematic	30
Figure 3.2 Relative wavelength shift measurement experiment setup	31
Figure 3.3 Narrow linewidth laser diode response for step up function	32

Figure 3.4 Narrow linewidth laser diode response for step down function	33
Figure 3.5 Demonstration of locating corresponding voltage	33
Figure 3.6 Sinusoidal Modulation of different frequencies	35
Figure 3.7 Narrow linewidth laser diode response for step down function	36

CHAPTER 1

INTRODUCTION

1.1 Background & Motivation

1.1.1 Current state of the art of acoustic emission (AE) sensors

AE is elastic waves typically in the range of frequency from 100 kHz to 1MHz. The AE sensor acts just like a highly-sensitive “ear”. The sensor converts AE signal to usable voltage signal. Additionally, embedded AE sensors help understand how structure interact in its natural setting. Most of the time AE is generated by damage-related structural changes, such as metal fatigue, structure crack initiation, and material breakage. Therefore, AE detectors are essential for the Structural Health Monitoring (SHM). An extensity, extreme sensitive, and reliable AE detection system is thus highly demanded.

Nowadays, AE detection market is dominated by ceramic piezoelectric transducers (PZTs). However, there are many pitfalls for PZT AE sensor: 1) High electric field can cause breakdown and failure; 2) it is inconvenient to embed the sensor into some structures; and 3) each sensor needs a pair of electronic cables for signal transmission. A Fiber-Optic AE sensor is brought in to provide an alternative solution.

1.1.2 Advantage of Fiber-optic Sensor

Fiber-optic AE sensors are one of the most promising techniques to address the abovementioned shortcomings [1]. Optical fiber based sensors have many excellent

qualities that offer advantages over electronic PZT sensors in the field of SHM. Most common optical fiber based sensors equip with a fiber Bragg Grating(FBG) structure on a fiber tip as sensor head. Optical fiber is made of durable silica glass with strong coating, is light, small, and flexible. These qualities allow it to be embedded in complexed structures with minimal effects to structural integrity. Unlike metals, silica is naturally corrosion resistant, therefore, such embedded sensors would be able to monitor a structure throughout their lifetime. Furthermore, due to the non-conductive nature of silica, optical fiber possess immunity to electromagnetic interference [2]. A distributed sensor array can be easily manufacture on an optical fiber, due to the excellent multiplexing capability of fiber, moreover, a single FBG region occupies only a very narrow bandwidth of a spectrum [1, 2, 3].

1.1.3 Challenge of fiber-optics sensors

Due to the advantages that addressed prior, FBG based sensors have recently been a subject of much interest for use as AE inspection sensors [4, 5]. Implementation of AE detection is through observing the AE-induced reflection spectrum shift. AE wave that impacting upon a FBG sensor causes a spectral shift in its reflected wavelength. Since the entire reflectivity spectrum shift with the reflected wavelength, locking the wavelength of a narrow-linewidth semiconductor tunable laser to a linear portion of the FBG reflection spectrum is used for intensity-based demodulation.

Unfortunately, traditional FBGs have inadequate sensitivity, due to the relative broad spectral slopes (~ 0.3 nm) [1]. A π -phase-shift FBG can greatly increase the sensitivity due to the ultra-narrow linewidth of the spectral notch in the reflection spectrum [1].

However, there are still many restrictions in many practical applications. Any kind of sensor is unavoidable subject to a low-frequency background strain arising from structural deformations and/or temperature variations. The large background strain, which is superimposed onto the AE signal and often significant larger, can easily drift the laser wavelength out of the linear range of the π FBG.

1.2 Chirped fiber-Bragg-grating Proposal

1.2.1 solution of the Challenge

Here, we proposed a fiber-optic AE sensor system based Chirped FBG (CFBG) sensor head, and laser-intensity demodulation method. This system is guided by smart feedback control for high-sensitivity AE detection under large low-frequency background strain. CFBG as a sensor head can realize both high sensitivity and accommodate large external strain. CFBG has unique spectrum profile which has a series of steep notches, resulting from two cascaded identical chirped grating structures. Multiple extremely narrow notches responsible for the enhanced sensitivity, and the broad spectrum range can accommodate the shifted caused by low-frequency large strain. When large strain applies to the sensor head, the notch drifts out of the tuning range of the laser, and a neighboring notch moves into the linear tuning range. Through a smart feedback control unit - which is the major contribution of this thesis - the narrow linewidth laser is unlocked from the current spectral linear region and relocked to the desired point of the new notch. The feedback control system is optimized to utilize fast speed of the unlocking/relocking process ensures that the AE signal is monitored without significant disruption [6, 7].

1.2.2 Thesis Structure

The aim of the thesis is to study the control theory and evaluate the experiment that is designed to free CFBG from low-frequency strain. It is organized as follows:

Chapter 1 contains the motivation and short history of AE sensor development. Chapter 2 introduces theories of the system, design specification based on optical characteristic, then implementation and evaluation of the smart control system. Also, the dynamic operation and time delay is analyzed thoroughly. Chapter 3 documents the laser characteristic in order to perform accurate tuning. Precise control parameters can be finalized at the end of the chapter. Chapter 4 includes a summary and a discussion about the future works that may follow the work that accomplished in this thesis.

CHAPTER 2

SMART FEEDBACK CONTROLLER

In order to design the control unit, the properties of different components in the sensor need to be studied comprehensively. Those components can be classified into three categories: 1) sensor head, which contains a CFBG structure; 2) laser controller and optical source; and 3) smart feedback unit.

2.1 Description of the Sensor System

2.1.1 Operation Principle of the Sensor Head

A regular FBG features periodic index perturbation to the fiber core over a certain length of the fiber, which results in the reflection of light at a particular wavelength called the Bragg wavelength λ_B , given by.

$$\lambda_B = 2n_{eff}\Lambda \quad 2.1$$

where Λ is the grating period, and n_{eff} is the effective refractive index of the optical mode supported by the fiber. The ultrasonic waves applied on the fiber grating area alter both the effective refractive index, via the elasto-optic effect, as well as the grating period [8]. Therefore, AE detection can be implemented by monitoring the spectral shift of the FBG.

According to Eq. 2.1 when Λ change a chirping sequence, there will be multiple reflectivity maxima in the grating range. The CFBG, whose reflective index vary along the grating length, can easily cover a larger wavelength range and can be adjusted flexibly by changing the chirp profile [9]. The sensor head consists of two cascaded identical CFBGs that forms a Fabry–Pérot interferometer, as shown in Fig. 2.1. Effective cavity length L_{eff} varies with wavelength λ . Since the two CFBGs are identical, therefore, the reflecting position for the two CFBGs are the same, and the distance between them are equal to cavity length L plus grating length L_{g1} . The formula for the neighboring peak interval $\Delta\lambda$ can be expressed in Eq. 2.2

$$\Delta\lambda \cong \frac{\lambda^2}{2\eta_{eff} \cdot L_{eff}(\lambda)} \quad 2.2$$

Since the effective cavity length stays the same for different wavelength, therefore, theoretically the notches are equally-spaced, as shown in Fig. 2.1.

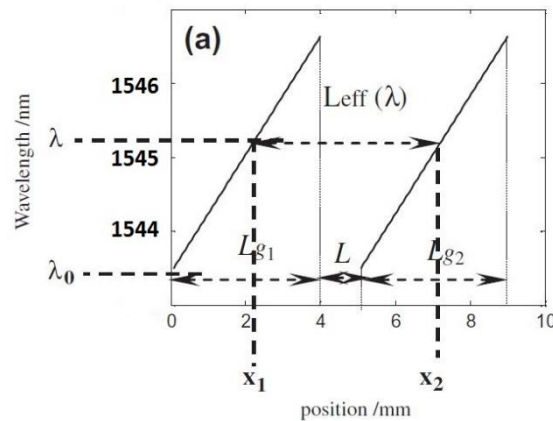


Figure 2.1 Effective cavity length L_{eff} changes with wavelength for identical chirped pair FP cavity [9]

The reflection spectrum of an identically chirped grating that is fabricated by UV light is shown in Fig. 2.2, and the distance between different notches that can be used for AE

detection are approximately equal. The laser output wavelength should stay on one of the most linear and steepest sections highlighted in red.

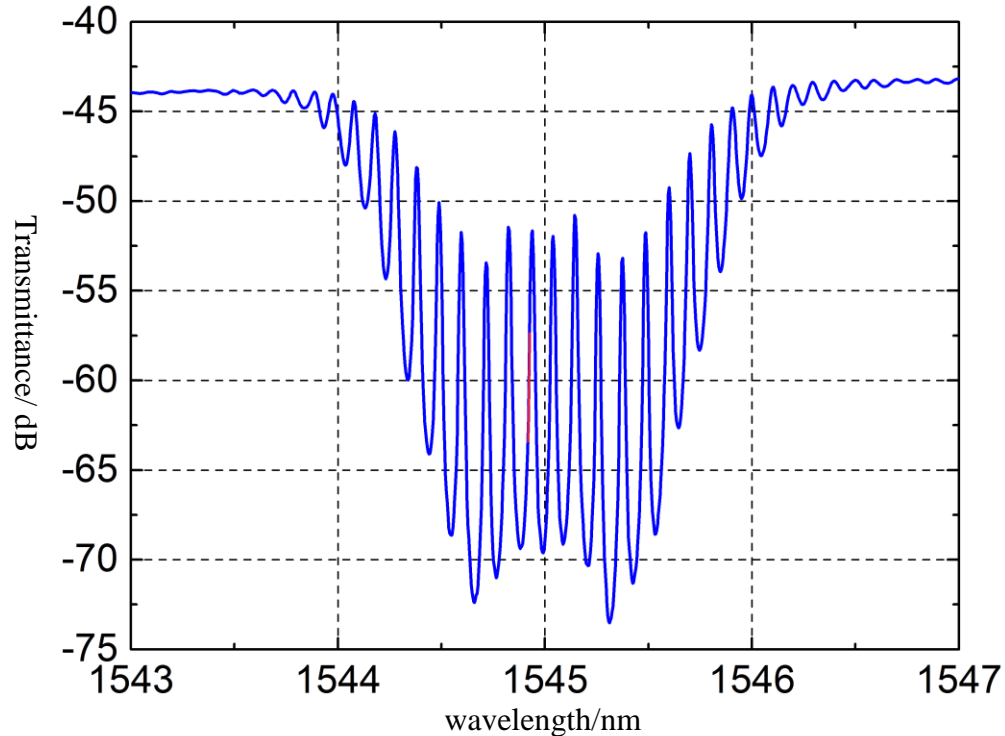


Figure 2.2 CFBG spectrum profile for this experiment

Intensity-based demodulation is a method that monitoring intensity changes of the reflectance of laser whose wavelength is locked to the slope of the sensor spectrum. Both background strain and AE wave can alter the reflectance intensity. However, only the strain from ultrasonic waves is desirable. Wavelength locking by a feedback controller is needed to tune the laser wavelength to follow the wavelength shift of the sensor from the background strain. The feedback controller acts like a low-pass filter, and it filters out the low frequency larger background strain for wavelength locking, and leave the high frequency AE signal behind. The controller constantly provides control signal to maintain laser wavelength on the linear region of a notch while undergoing background strain.

Here is an example shown in Fig. 2.3 about intensity-based demodulation, laser wavelength is locked on the linear range, indicates as the orange arrow. According to the figure, when the spectrum alters with AE vibration horizontally, and the laser wavelength stays the same, therefore, reflection intensity of laser is changed by AE waves.

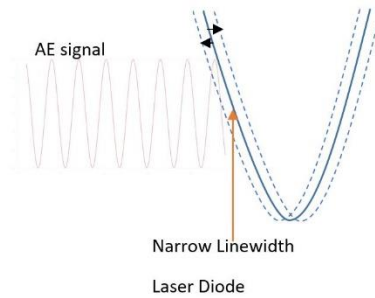


Figure 2.3 Example of laser intensity-demodulation

2.1.2 Laser and Laser Controller

Narrow linewidth monolithic coherence laser diode (EP1550-NLW-B-100) is used as narrow light source whose wavelength can be tuned in high speed through current injection. The linewidth for this laser is extremely narrow see Fig. 2.4(a). The intensity and wavelength increases linearly with injection current after lasing threshold show in Fig. 2.4(b). More details on mechanism and tuning characteristics of the laser will be discussed in Chapter 3.

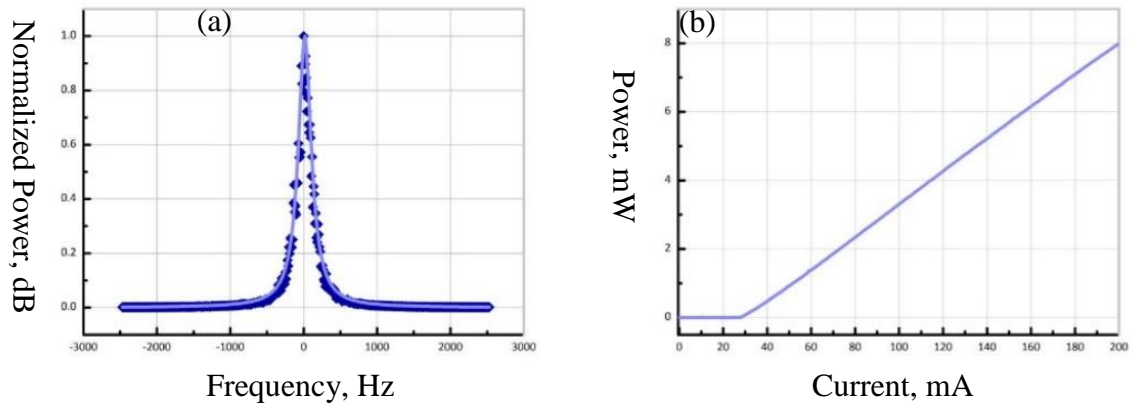


Figure 2.4 (a) Linewidth of the narrow linewidth laser

(b) Theoretical photon intensity has linear relation with current [11]

2.1.3 Role of the smart feedback control unit

As mentioned above, a feedback controller applies in the system, and “filter” the low frequency background strain out, thus the laser can stay on the linear slope. However, when the strain is large enough to move the wavelength out of the laser tuning range, meanwhile, the spectral notch at the longer wavelength drifts into the tuning range and becomes available for AE detection. The laser is then quickly tuned to the next notch and locked at its spectral linear slope, and the procedure is governed the smart feedback control units, so that AE can be monitored without significant disruption.

2.2 Design of the smart feedback control unit

In order to design the smart feedback control unit, the partial-integral (P-I) feedback controller theory has to be studied first. Then integration between P-I controller, and

smart controller will be discussed, finally, all the necessary electronic design is documented in detail.

2.2.1 Partial – Integral (P-I) Feedback Controller

As prior mentioned, P-I controller is deployed to implement locking wavelength on the linear region of a notch. A commercial P-I feedback controller is used in the system (Model LB1005, New Focus), and it contains three major parts in the system show in Fig. 2.5. Each one needs to be configured correctly in order to perform the locking/unlocking procedure. First one is a difference amplifier, it receives 5% of the light injected to a photodetector (PD1) as feedback control signal. This signal is to add offset adjust voltage and minus normalization signal yields the desired process value, known as error signal (V_{error}). This value is fed into the P-I filter, and the output of P-I filter is depended on the gain value. The output is just simply a sum amplifier, and it sums the control signal with the modulation signal (MOD signal) [12]. Take a closer look to each component:

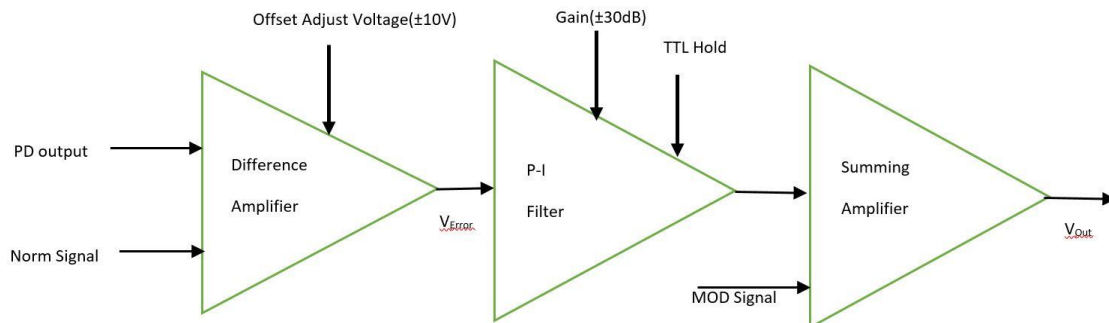


Figure 2.5: Feedback Controller System Block Diagram

1) Difference Amplifier

Error signal is expressed as

$$V_{Error} = V_{in} - V_{norm} + V_{offset}, \quad 2.3$$

which can be used to determine the locking point. Error monitor signal is equal to target voltage (locking point) minus the input voltage. The goal of partial integral feedback system is to limit the error signal to zero by sending back the feedback signal.

2) P-I Filter

P-I filter is the core of the feedback control system, and the locking mechanism is implemented by a P-I Feedback Controller. We can write the transfer function in time domain in Eq. 2.4. Convert it into frequency domain, we get Eq. 2.5. In our application, plug $T_I = 2\pi f_{PI}$ into Eq. 2.6, we get equation. User can adjust to Gain K (amount of proportional gain) to optimize the PI system. That will affect to both the integral and proportional control part.

$$u = Ke + K \int e \quad 2.4$$

$$C(s) = K(1 + \frac{1}{T_I S}) \quad 2.5$$

$$V_{Control} = V_{Error} + \frac{K2\pi f_{PI}}{s} (1 + \frac{s}{2\pi f_{PI}}) \quad 2.6$$

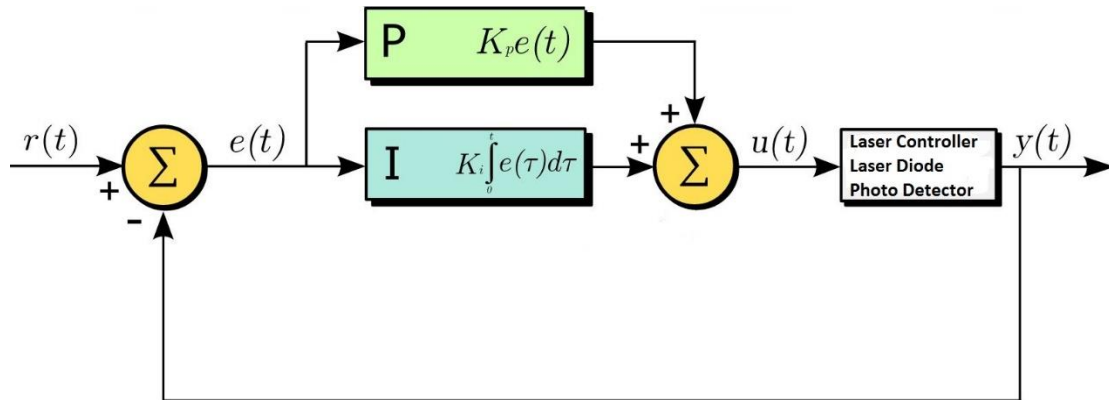


Figure 2.6 A Partial Integral System [13]

There is a deactivation/activation signal input on the servo controller, it is called TTL signal, it is a high-low digital signal, when we give the servo controller a logic high voltage, the loop will open (deactivate), and a logic low TTL signal will close (activate) the loop.

3) Output Signal

The controller output signal is the summation of control signal and modulation signal. The signal contains proportional-integral (P-I) filter output, sweep signal, and modulation signal. This output has an impedance of 50Ω and a drive current of $\pm 20 \text{ mA}$. Output signal is directly connect to laser controller modulation input BNC port.

2.2.2 Smart Feedback Controller

The smart feedback not only includes the P-I feedback controller, but also has a unit with two functionalities: 1) locking/unlocking mechanism; 2) signal normalization.

Locking/unlocking mechanism:

The smart feedback control unit will provide an unlocking signal followed by a modulation voltage. These two signals are designed to unlock the old locking point, and locate the new locking point. An example is given in Fig. 2.7 as the laser wavelength getting near to the upper limit of the laser tuning range, the next spectral notch at the shorter wavelength moves into the tuning range because the FSR of the CFBG sensor designed to be smaller than the laser tuning range. The laser is then unlocked from its previous notch, its wavelength is tuned to the lower end of the range, and the laser is relocked to the new spectral notch for continuing ultrasonic detection.

Signal Normalization:

A scenario shown in Fig. 2.7(a), the “jumping” process through the spacing is governed by modulation signal, indicated as the orange line in the figure. Note that the injection current not only tunes the laser wavelength but also modulates the laser power. Since our P-I controller locks on certain optical intensity of laser reflection, the P-I will find a new point that has the same reflection as the old locking point, indicated as a yellow dot in the

figure. Unfortunately, the new locking point will not be in the linear range of the notch on the left. This will dramatically decrease the sensitivity of the sensor.

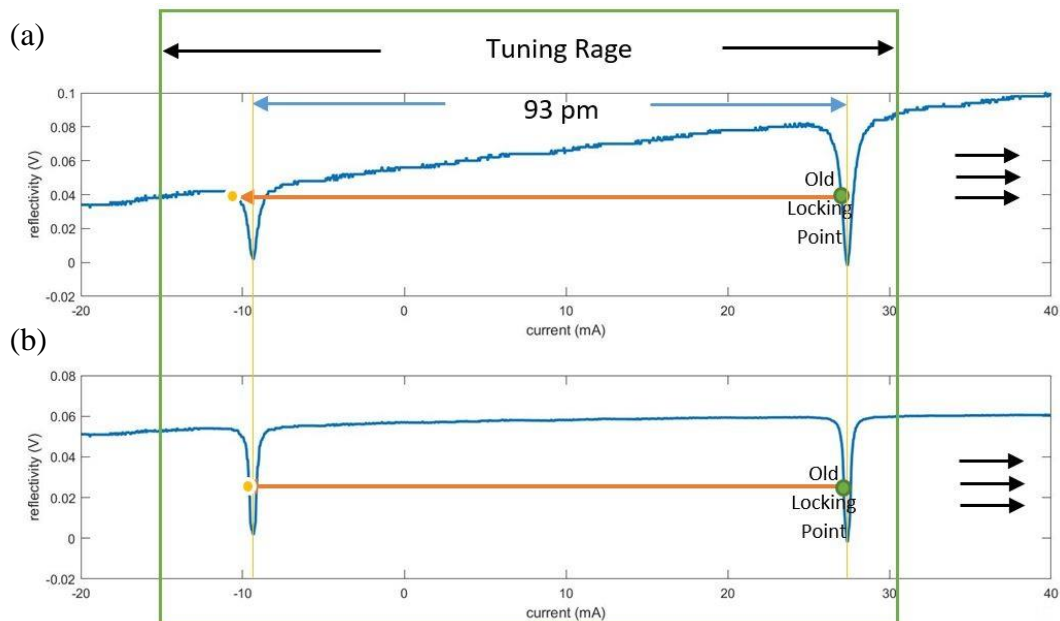


Figure 2.7: Demonstration of seeking new locking point

A circuit made by op-amps has been designed, and it provides a compensation signal to “flatten” the ramp. This signal is a superposition of an inversed laser intensity’s fraction and an offset voltage. Since the normalization signal can be directly coupled into AE signals, great effort has been put to reduce the noise by 1) designing a common ground that is a direct physical connection to the Earth; 2) designing the op-amp to have a high input impedance(ideally infinite) and low output impedance (ideally zero) by a voltage follower. Finally, after the normalization, the reflectivity spectrum for the CFBG is displayed in Fig. 2.2(b). After normalization, narrow linewidth laser wavelength can be locked on the linear region of the previous notch shown as yellow dot in the figure without reset the locking voltage.

2.2.3 Modulation signal design

The unlocking/locking process (“jumping”) is guided by modulation signal V_{MOD} , the modulation signal is not a simply delta function, instead, it has trapezoidal shape, as shown in Fig.2.8.

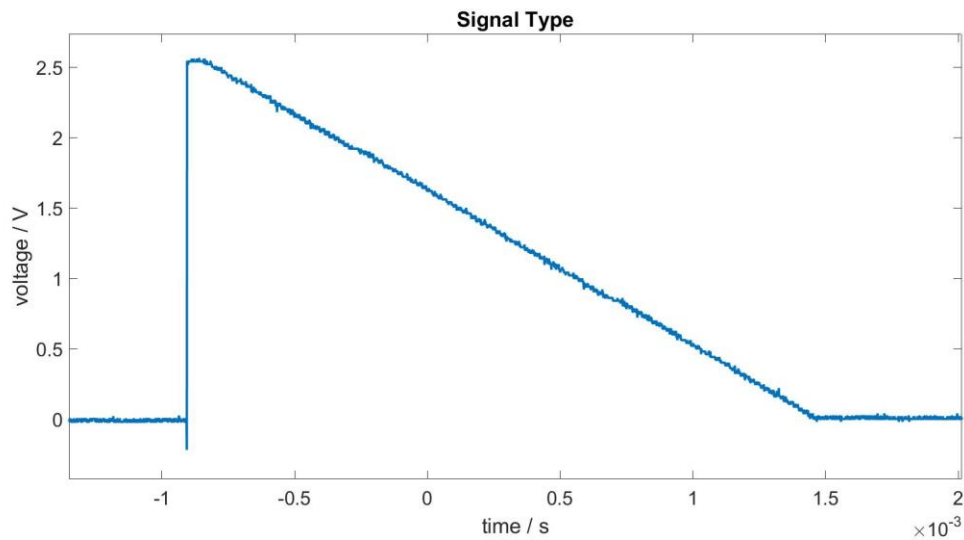


Figure 2.8 Example of a Modulation Signal

The ramp signal significantly delayed the locking/unlocking procedure, but ramp signal is essential, because the response of narrow linewidth laser is slow. The ramp signal is designed to guide laser to the correct locking-wavelength. If the V_{MOD} signal is delta function, the laser would not have time to move over spacing sufficiently large wavelength range. Otherwise, the laser was not able to regain locking.

During the “jumping”, the microprocessor continuously monitored the laser current, but it will not give another V_{MOD} signal until the previous signal has totally ramp back to zero.

Otherwise the feedback controller will not give the right voltage signal to find the next notch correctly.

2.2.4 Implementation of Modulation Signals

We need at least four independent parallel general-purpose input/output (GPIO) lines. In our application, one line is used to generate the modulation signal (V_{MOD}); one line is assigned to generate TTL signal that can unlock the servo feedback controller; one line is the analog-read line, and this line continuously monitor the laser current; and another line is used for user interface designing.

V_{MOD} looks like a trapezium, the design reasoning is stated above. The signal is implemented by concatenate three linear function in the microprocessor, and the slope is reconfigurable for different CFBG tuning. TTL signal is simply implemented by a pull-up signal, and it's held high for a short delay, and follow by a pulldown signal. Once again the width of the TTL is reconfigurable. Push-buttons can generate raising/falling edge function, and the signal can be used to control the status.

As mentioned about, smart controller is required to operate three major functionalities: 1) providing control signals, 2) supplying normalization signal, and 3) user interface. Arduino DUE development board is capable of these tasks. It has ultra-low power consumption, and can be easily powered by a battery. The development board is equipped with Atmel SAM3X8E ARM Cortex-M3 CPU, and sufficient flash memory, which can store a large lookup table. It is the first Arduino board based on a 32-bit ARM core microcontroller. It

has 54 digital input/output pins (of which 12 can be used as PWM outputs) [14]. Since there is no edge for laser current, edge-triggering interrupt cannot be used. So, the 84 MHz main clock is utilized as timer to provides interrupts, analog read is executed within timer interrupt. The speed of microprocessor will be analyzed in the end of the chapter.

2.2.5 Digital to Analog Converter

There are two options to provide analog signal. Arduino generic Digital-to-Analog Converter Controller (DACC) offers up to 2 analog outputs, making it possible for the digital-to-analog conversion to drive up to 2 independent analog lines. However, we decided to not use the generic DACC, because it takes 25 clock periods for DACC to update the analog output. In contrast, parallel digital output is much faster, because from previous experience, the parallel digital output can reach as high as 4 MHz. That's the reason a peripheral parallel DAC.

The DAC0808 is an 8-bit monolithic digital-to-analog converter (DAC) featuring a full-scale output, with current settling time of 150 ns (6.6MHz bandwidth) while dissipating only 33 mW with $\pm 5V$ supplies. Output range of the digital-to-analog converter is depending on voltage supply V_{cc} and digital reference voltage V_{EE} . When the $V_{cc} = 12 V$ and $V_{ee} = -5V$, the output current is -2 mA. Consequently, concatenating an appropriate op-amp to the DAC can convert the current output to desired voltage output V_{MOD} , Show in Fig. 2.9.

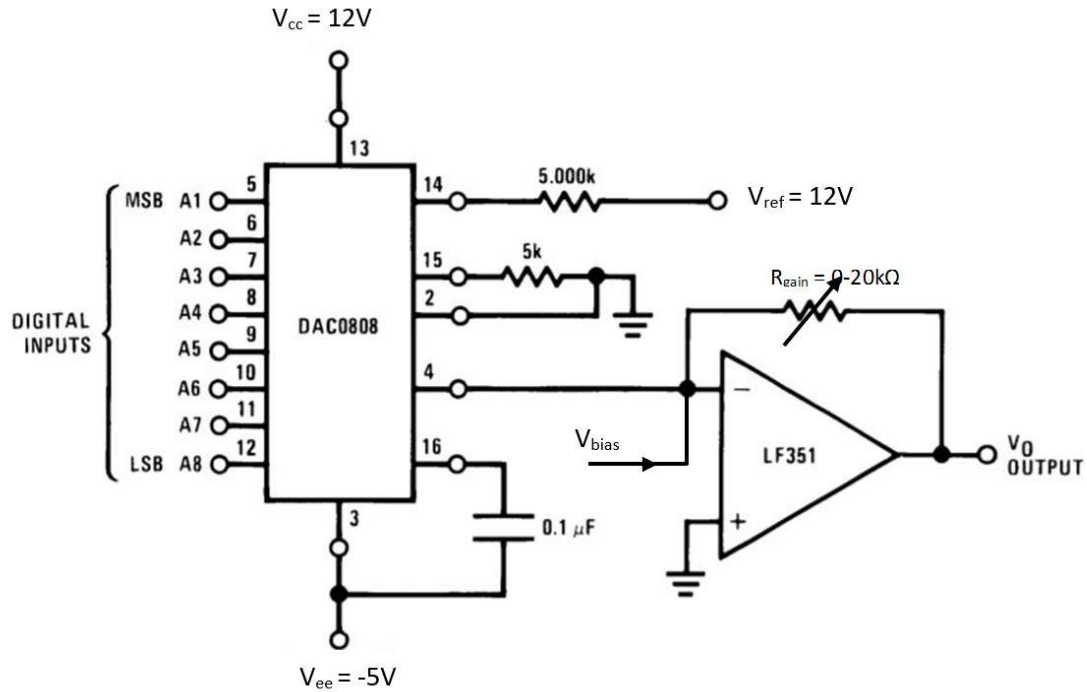


Figure 2.9: Digital - to - Analog circuits schematics [15]

2.3 Experiment Demonstration

As previously mentioned, there are three major components in this system, control system, sensor head, and laser. The sensor system is shown in Fig. 2.10; different components are labelled in different color.

2.3.1 System Setup

Optical source: original equipment manufacturer (OEM) laser controller housing and narrow-linewidth laser diode, are illustrated in blue blocks. Feedback control system is a combination of a P-I controller, and micro-processor control unit, and they are shown in the green blocks. Sensor head is embedded on an aluminum plate, marks in grating shape. Yellow blocks indicate peripheral circuits, and orange blocks designates optical devices.

Scanning method is governed by a low frequency triangle wave, and its response reflectance intensity is illustrated in Fig. 2.11. Scanning triangular signal is provided by the microcontroller, and it will be turned off when the system is locked. Normally, a larger scanning voltage is applied to allocate which notch we want to lock on. After that, reduce the voltage and adjust the center wavelength to “zoom into” the notch detail. We find the linear region of the notch that has the deepest slope. Setting locking point can be done by adjusting the V_{offset} equal to the voltage of desired locking point. Desired locking point is illustrated as the green dot and the voltage level is shown as yellow dash line. At this point $V_{in} - V_{norm} = V_{offset}$, and difference amplifier operates $V_{Error} = V_{in} - V_{norm} - V_{offset}$, that yields $V_{Error} = 0$.

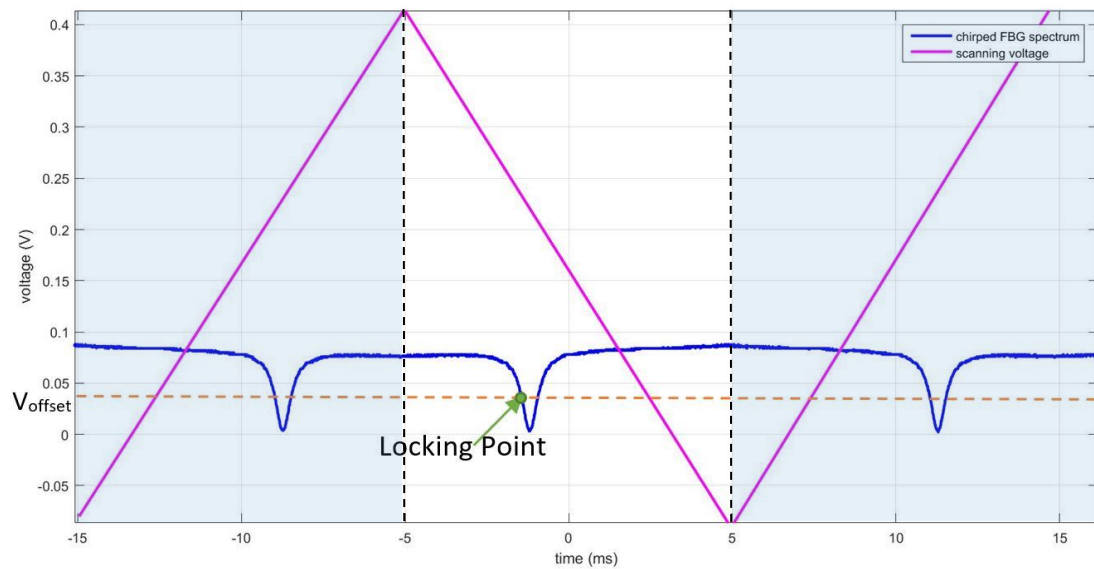


Figure 2.11 finding locking point using scanning method

In practice, it is better if there were only one notch within half period of the scanning signal, otherwise it will lock on the one that is closest to the sweeping center, which can be ambiguous sometimes. Since each rising or falling scanning signal scans through the

same notch, we only consider the middle spectral notch, indicates in the white region in the figure.

2.3.3 Locking

There are many notches that can be used for AE detection, and they have different spectral width, and slightly different spacing. In our experiment, six narrowest notches in the center were used for AE detection, and the sensitivity of each notch was evaluated. The results are shown in Fig. 2.12. Note, all the notches are locked on the same reflectance intensity. As expected, narrower spectral notches lead to large response. In the following section, we demonstrate switching between different notches with minimum disruption using the smart control unit. When the sensor stretches, the spectrum moves towards the longer wavelength. On the other hand, when the grating area is compressed, the notch shifts towards the shorter wavelength. So, when sensor stretches,

we want to unlock/relock (“jump”) towards shorter wavelength, if sensor compresses, we want to jump toward longer wavelength.

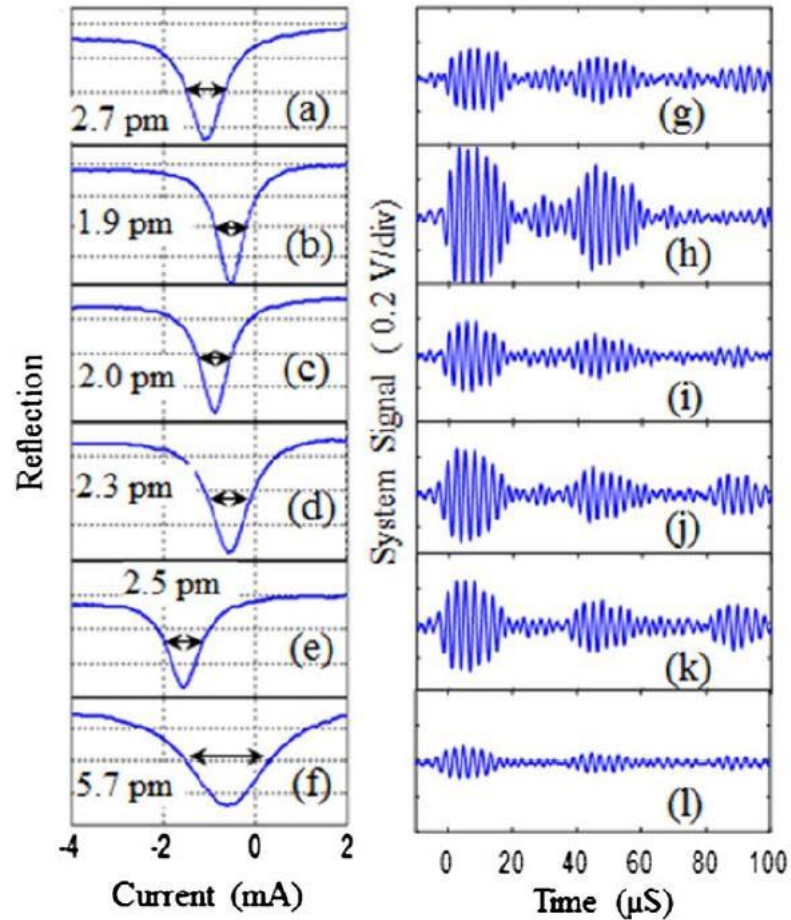


Figure 2.12 (a)–(f) Reflection spectra of the five spectral notches used for AE detection; corresponding (g)–(l) AE signals

2.3.4 Jump Towards Longer wavelength

The detailed operational procedure is illustrated in Fig. 2.13 (a) and (b), which show, respectively, the TTL signal, and the MOD signal. The entire procedure is segmented into three stages: 1) locking deactivated, 2) locking activated; and 3) reaching steady state. In order to illustrate the dynamic process, 10 points have been sampled from different

stages, as labeled in Fig. 2.13 (d). After the control system is unlocked known, indicated by the yellow line at t_0 , the modulation signal is then fed in, and error signal raises up from zero, as shown in Fig. 2.13(c). Looking closely, there is a small notch before point ①, which is caused by the laser output wavelength scanning through the spectral notch. Continuously driven by the modulation signal, the laser wavelength moves from point ① to point ④ very rapidly, as shown in Fig. 2.13 (d). In figure 2.13 (e), we can see, point ④ is almost located to the midpoint of the spacing between the two notches. After reaching the mid-point, TTL signal was set to low, and the smart feedback control system goes into stage two. Now the error signal is positive, that means the working wavelength is not on the locking point. Thus, the feedback loop is going to try to find a new point that yields zero error signal.

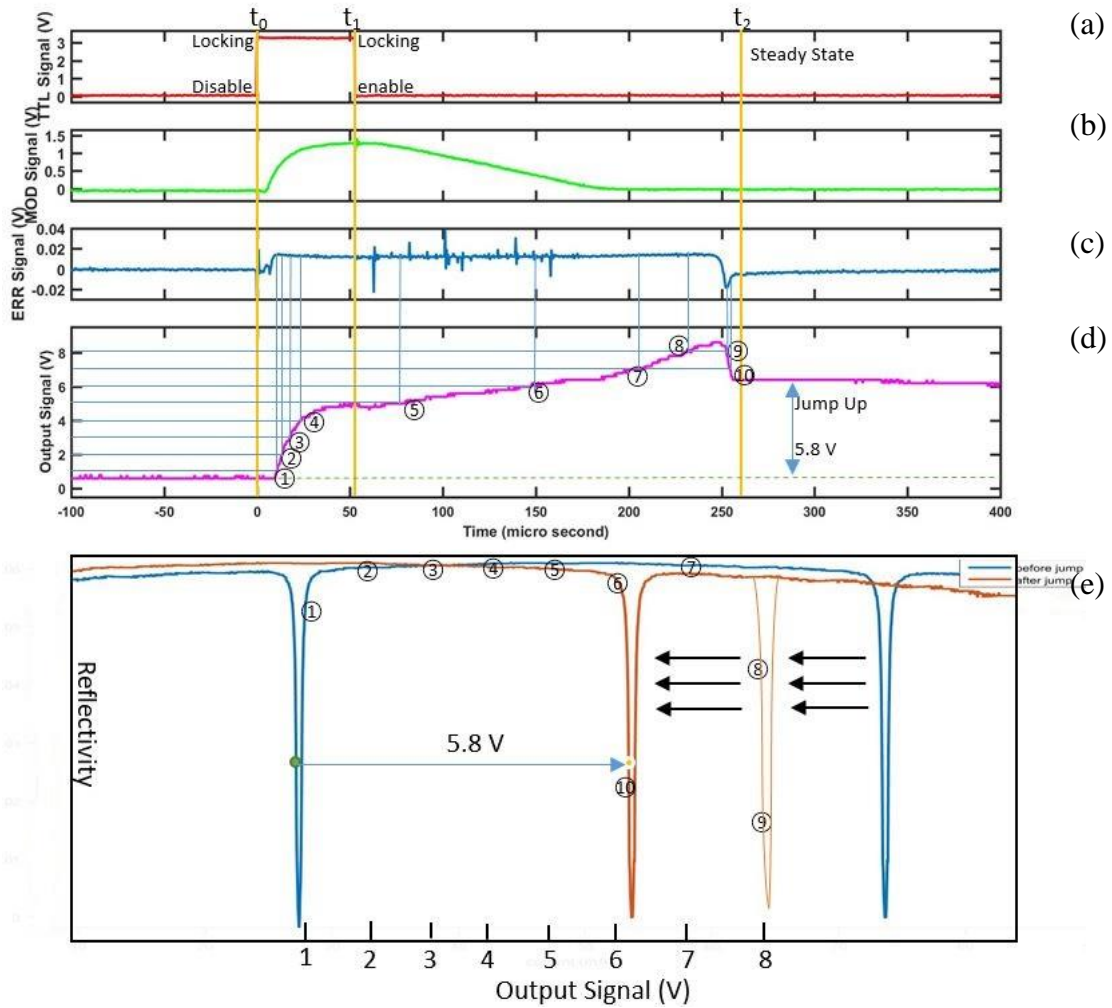


Figure 2.13 Control and monitor signals of the smart feedback control unit when the sensor was compressed

Recall the error signal $V_{Error} = V_{in} - V_{norm} - V_{offset}$, in this case, V_{in} is superposed by the optical feedback control signal and V_{MOD} signal. V_{norm} is used to cancel the intensity increase of the current injection, therefore, we can ignore this element. Now the $\Delta V_{error} = kV_{MOD}$, and it is a positive voltage, therefore, the feedback controller will seek for a wavelength on the spectrum that has less reflectance, thus the V_{in} can be lowered, and then V_{error} can drop down too. With the help of the “ramp signal”, the feedback system slowly moves the laser wavelength from point ④ to ⑥. When the wavelength reach to point ⑦, where locates in the region of next notch. The slowness is caused by low tuning

bandwidth of the laser; more analysis will be discussed in Chapter 3. After that point, the longer wavelength generates weaker reflection, thus, the feedback controller provides higher voltage to decrease V_{in} . Therefore, V_{error} signal can approach zero, and it is desired. After a short delay, V_{error} start to decrease after point ⑧. However, overshooting can be observed during the process, indicated by error signal dropping to sub-zero, illustrated as point ⑨. Coming up with a decline of injection current, and injection current drives the locking point to the left along with the drifting CFBG spectrum (point ⑨ to ⑩). After point ⑩, V_{error} settle to zero, and declares a complete unlocking-relocking process, which is stage 3. Total time-elapse ($t_2 - t_0$) is 220 μ s, and that makes the bandwidth for the demodulation system 4.3 kHz.

2.3.5 Jump to the Shorter Wavelength

The result indicates in the Fig. 2.14; the same theory applies to jumping towards the shorter wavelength. When the feedback system is unlocked, and wavelength is modulated by the V_{MOD} The laser wavelength decreases rapidly with the negative modulation signal. Thus, the grating reflectance drops, and the error signal raise up. Shows in region ① to ⑤. There is a narrow notch in the error signal between point ⑤ and ⑥, caused by the laser wavelength passing over the notch. After the wavelength passing the notch on the left. The reason for forcing the laser wavelength pass the notch peak is that, in the configuration used in our experiment, the P-I control can only seek locking point from the shorter wavelength end to longer end. It takes notable time for the wavelength goes

from point ⑦ to ⑧. Compare with “jumping up”, “jumping down” require higher voltage
Total time-elapse ($t_2 - t_0$) is 750 μ s, and it’s much slower than “jumping up”.

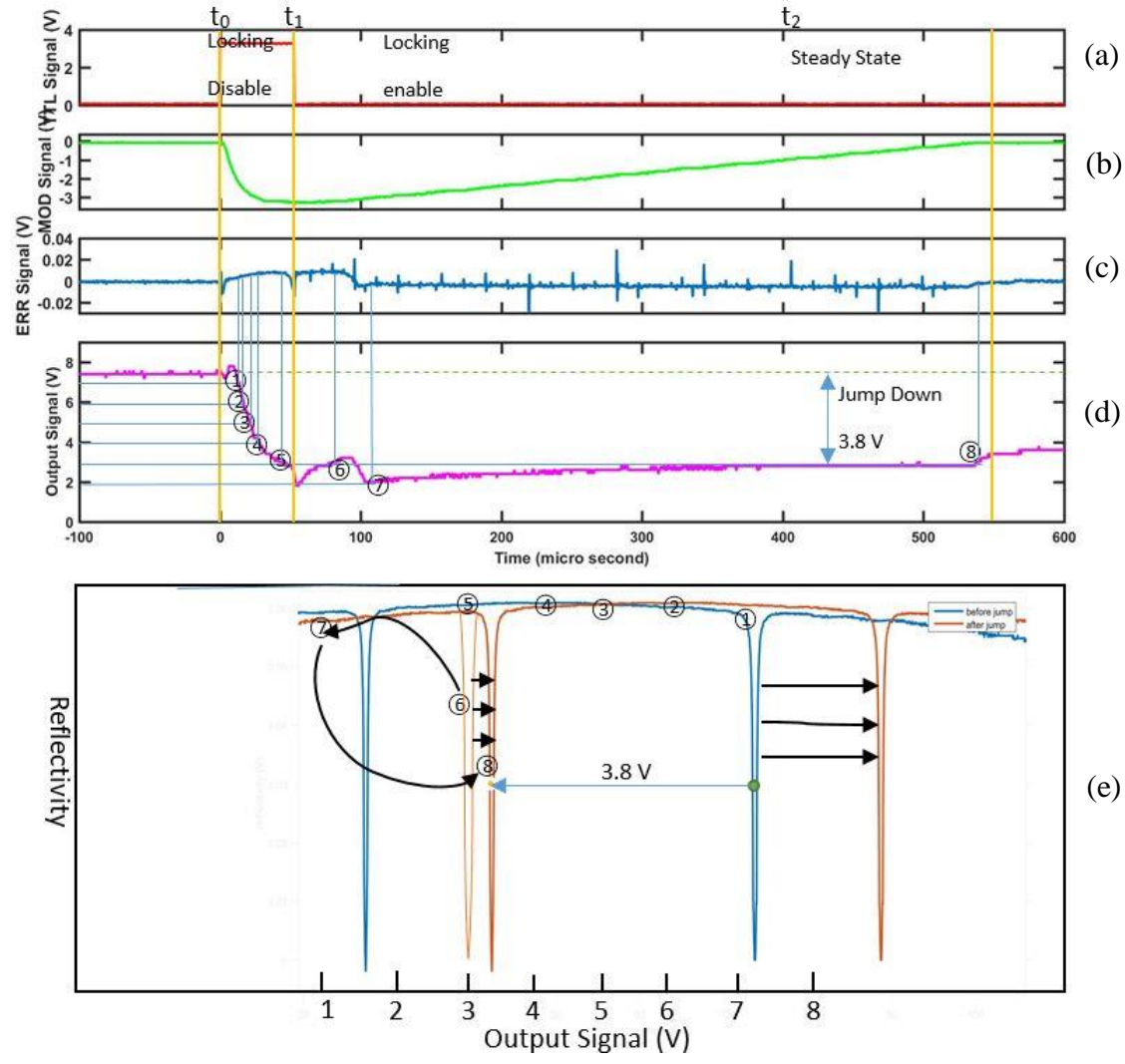


Figure 2.14 Control and monitor signals of the smart feedback control unit when the sensor was extended

2.4 Instrumentation

A portable instrument was developed by placing the smart control system including a servo controller (LB1005, Newport), light source, photodetectors, and power supply, in a

box . On the front panel, there is an optical signal input, and it connects to the CFBG sensor tip. Also, two electrical signal outputs, they are 1) error monitor that inspects the operation of the controller, and 2) AE signal output. Also, include a system on/off button to turn on/off the entire sensor system, a scanning button that enables the microprocessor triangle wave output. A V_{MOD} signal enable button that enable monitoring laser output signal, and giving “jumping” signal. Note, scanning mode and Mod enable mode shares use different timer interrupt, therefore, if one is activated, and the other one will be disabled. Two LEDs indicate the status of the system.

2.5 Summary

CFBG sensor head with a smart feedback control was setup and demonstrated AE detection on an aluminum plate under large low frequency background strain that is provided by a shaker. The reflection spectrum of the sensor has six narrow notches within the broad reflection bandwidth that can be used for laser-based intensity-demodulated AE detection. The optical source was an inexpensive semiconductor laser whose wavelength can be tuned in high speed, through current injection, over a range larger than the FSR of the CFBG. The smart feedback scheme was designed to select and lock the laser line on the desired operation point of a spectral notch that fell in the tuning range of the laser diode. Finally, this system is packed into a costumed case, for portable AE detection.

CHAPTER 3

CHARACTERIZATION OF NARROW LINEWIDTH LASER

In this chapter, we study the wavelength tuning of the semiconductor laser.

3.1 Mechanism of Laser Wavelength Modulation

As mentioned above, laser is tuned by current injection. Current injection tunes the laser wavelength through two independent mechanisms: carrier density and temperature.

For laser with cavity length of L and effective refractive index of n , the angular frequency of the laser output is given by

$$\omega = \frac{m\pi c}{Ln_e} \quad 3.1$$

$$g_{mod} = \frac{1}{L} \ln\left(\frac{1}{|r_1 r_2|}\right) \quad 3.2$$

where m is the order number of the cavity mode and c is the speed of light in vacuum.

Refractive index (n_e) change, which is induced by temperature and injected carrier density, plays an important role of wavelength tuning [23].

3.1.1 Measurement of Wavelength Tuning

. In this section, the tuning performance of the narrow linewidth laser (Model number) used in our experiment is studied by considering the following situation:

- (1) Response of the laser wavelength to a step change in injection current.
- (2) Response of laser wavelength to sinusoid current modulation.

Mach–Zehnder interferometer (MZI) was used as the “ruler” for measuring wavelength shift.

3.1.2 Theory of Mach–Zehnder Interferometer(MZI)

The schematics of an unbalanced MZI is shown Fig. 3.1. Through a fiber-optic coupler, the light is split into two arms. with one arm having a much longer path than the other. The lights from two beams are then recombined together through another coupler.

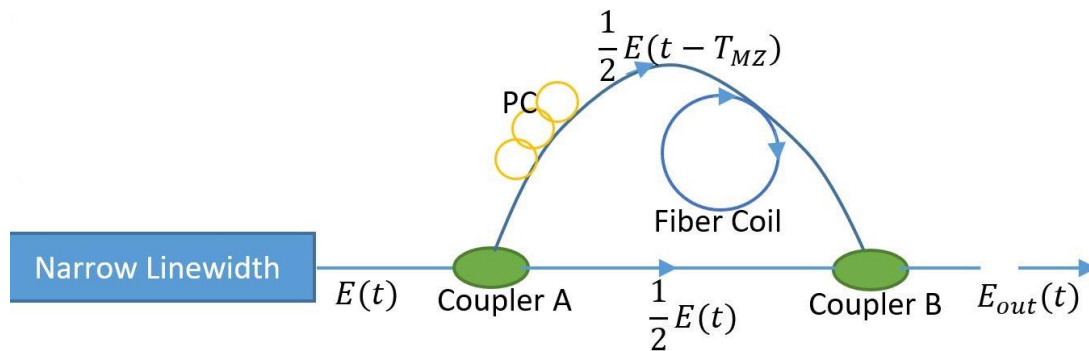


Figure 15 Fiber Mach–Zehnder interferometer Schematic

The interference between the two beams leads to interferometric fringes with a free-spectral range (FSR) given by

$$FSR = \frac{c}{\Delta L_{MZ} n}$$

where L_{MZ} is the path length difference of the two arms, and n is refractive index of the optical fiber core. We have built an imbalanced MZI with an FSR of ~ 4.8 pm.

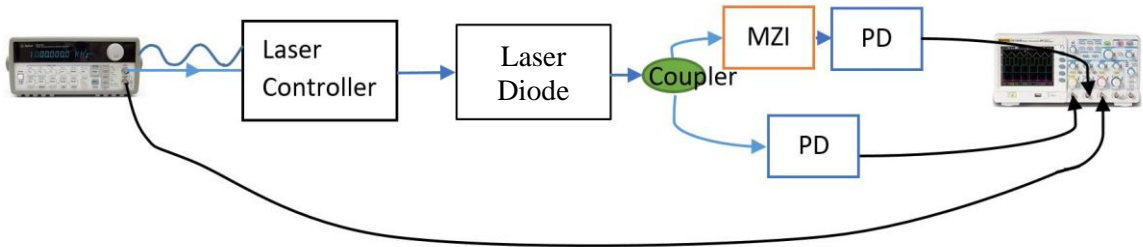


Figure 16 Relative wavelength shift measurement experiment setup

3.2 Measurement setup

As shown in Figure 3.2, a function generator provides a sweep sinusoidal signal to the laser controller for pure frequency modulation. Through a fiber coupler, part of the laser output goes through a MZI and is detected by a photodetector (PD). The rest of the laser output goes to another PD to monitor the optical power of the laser, which will be used to normalize the MZI signal. In an oscilloscope or a data acquisition unit, the signals from both PDs as well as the sinusoidal signal from the function generator are monitored and displayed.

3.2.1 Response to Step Current Modulation

First, we measured the wavelength shift as a function of time when the laser is modulated by a step change of injection current. Because a high time resolution measurement over a relative long period time is required to capture the signal from the MZI, a data acquisition (USB-6366, National Instruments) is used to collect both the step function, and the MZI fringe signal.

Fig. 3.3 (a) shows the signal from the MZI Figure 3.3(b) shows the wavelength shift vs. time as calculated from Fig. 3.3(a), when the laser wavelength jumps toward longer wavelength. Fig. 3.4 shows the results for the case when the laser wavelength jumps toward shorter wavelength by a step function of the same step amplitude for “jumping down”, the wavelength shifted by a total of 140 pm and it takes 8.7 ms to reach 80% of the total wavelength shift. For “jumping up”, it was 2.12 ms which is faster than “jumping down”. There is 7 pm difference in the total wavelength shift between step up response and step down response.

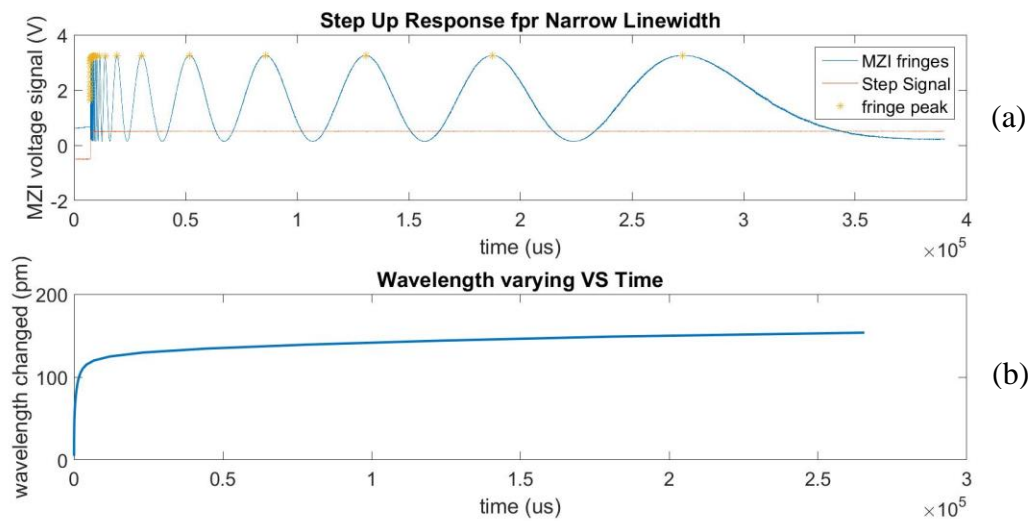


Figure 17 Narrow linewidth laser diode response for step up function

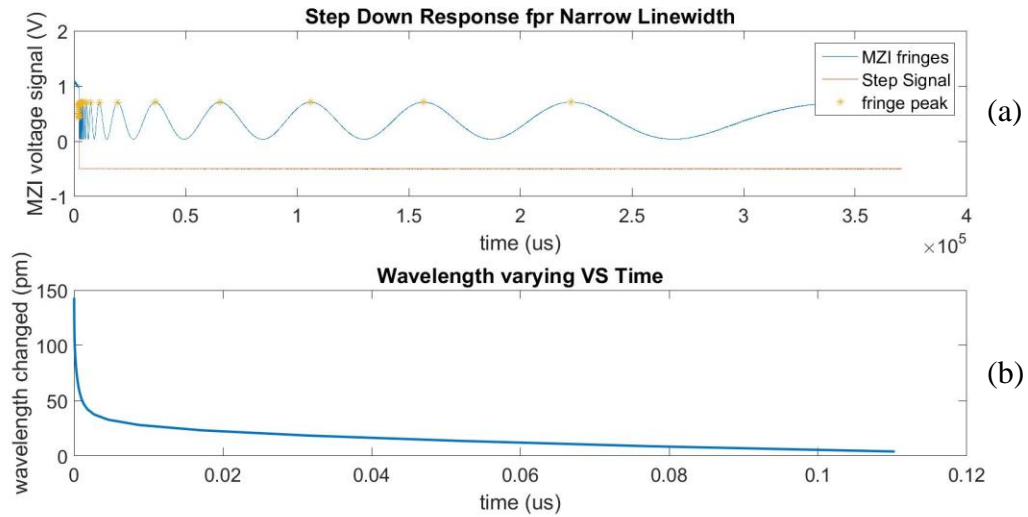


Figure 18 Narrow linewidth laser diode response for step down function

3.2.2 Sinusoidal Modulation

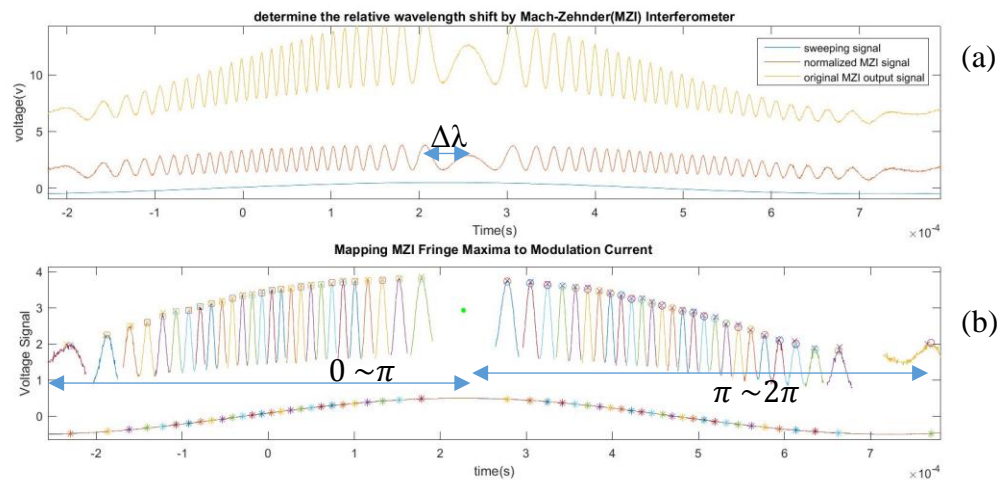


Figure 19 Demonstration of locating corresponding voltage

Fringes that generated from MZI illustrated in Fig. 3.5(a) when the frequency of the sinusoidal modulation was 1kHz. The sweeping signal can be divide into raising period $0 \sim \pi$, falling period $\pi \sim 2\pi$. A symmetric point can be observed in the spectrum, that indicates the turning point of scanning signal. At that point, the modulation current isn't enough to cover the spectral width, then it starts to roll down. This point can help us find

the corresponding modulation current for each fringe peak. Firstly, we want to distinguish the symmetric point and MZI fringe peaks due to the prominence difference. Then the symmetric point of spectrum is aligned to the peak of the sweeping signal, and it is indicated as a green dot in Fig. 3.5(b). In this circumstances, we assume the last wavelength displacement (shown as $\Delta\lambda$ in figure) in $0 \sim \pi$ and $\pi \sim 2\pi$ are the same. This is the reason why all the “ellipses” in Fig. 3.5 have more linear top region. Next step is locating the corresponding modulation current for every constructive interference, indicated in Fig. 3.5(b). We take a whole the data of fringe segment (indicates in different color segments), and peak indicates as ‘x’ in the figure. Apply Gaussian curve fitting towards fringe notches. Then find the peak (shown in the circles), and map them to the sweep signal shown in blue color in Fig.3.5 (a).

Take mapped points on sweep signal and convert the voltage signal to modulation current, plot it against wavelength response. Note, wavelength is given by number of fringes multiplied by FSR (4.8 pm). See as Fig. 3.6, the wavelength responses are not linear, instead, the response looks like closed ellipse loops. However, when the frequency is low and high there the loop is relative more linear. In the figure, $0 \sim \pi$ modulation corresponding to the lower half of the “ellipses”, and the $\pi \sim 2\pi$ correlate with the upper half.

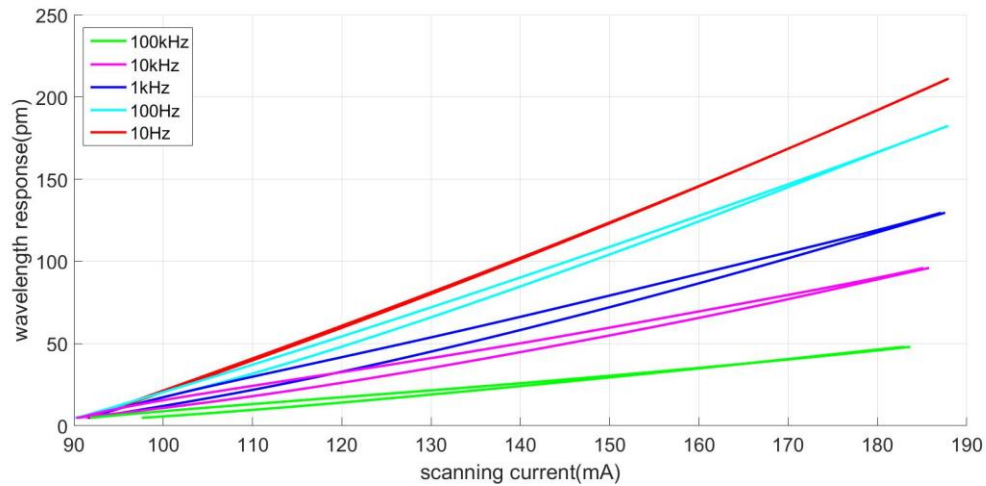


Figure 20 Sinusoidal Modulation of different frequencies

Sinusoidal current modulation and triangular current modulation yield different results; therefore, it's believed that this phenomenon is not caused by mode hopping [20, 22]. Instantaneous junction temperature changes the refractive index of the junction material and therefore varies the effective cavity length. The thermal factor makes a large impact in injection current tuning, except at high modulation frequencies. That's the reason why the frequency is high, the upper-half is less diverged from the lower-half. Therefore, in conclusion, the thermal inertia affects the frequency modulation [19].

It's worth mentioning in Fig. 3.4, the wavelength response for the lowest frequency(10Hz) is about four times larger than the highest frequency. More experiments are conducted to study frequency modulation (FM) responses for the narrow linewidth laser. Function generator provides 100 mA peak-to-peak sinusoidal current modulation, and the following frequencies are tested: 10 Hz, 75Hz, 100Hz, 500Hz, 1kHz, 5kHz, 7.5kHz, 10kHz, 50kHz, 75kHz, 100kHz.

Wavelength tuning range is determined by total number of the fringes covered by the modulation signal. Figure 3.7 shows the magnitude of the wavelength shift caused by a 100 mA peak-to-peak current modulation at different modulation frequencies and its linear fitting line. Note that the modulation frequency is in logarithmic scale. The dominant mechanism for the wavelength tuning is temperature modulation from the injection current. Previous study [23] shows that for a modulation frequency in the range of 0 Hz to 1MHz, the response of the laser frequency (or wavelength) modulation due to the temperature modulation is several times larger than due to carrier density modulation. [21,24].

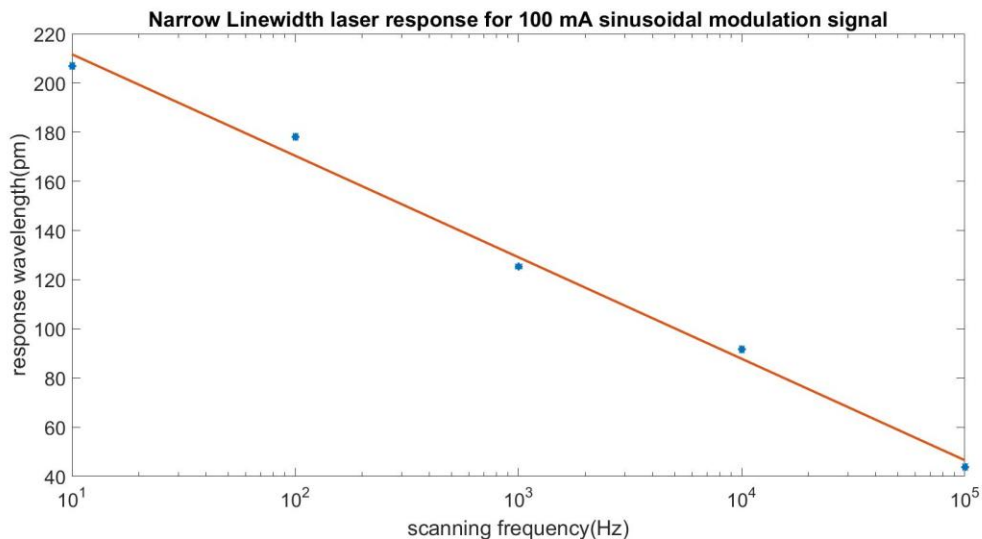


Figure 21 Narrow linewidth laser diode response for step down function

3.3 Summary

After studying the characteristics of the laser diode, the result can be used for accurate modulation. Step function response can help us understand the time needed to change the

laser wavelength over a certain range. Besides the applications of the diode laser in AE sensor system, the laser can also be used for wavelength demodulation of other optical sensors. The characterization of wavelength shift caused by sinusoidal current modulation may be used for accurate measurement of the optical spectrum of the sensors.

Chapter 4

CONCLUSION

4.1 Summary

This thesis summarizes the work related to the laser wavelength locking and wavelength tuning characteristics of a diode laser used in a fiber-optic AE sensor system based on a CFBG sensor head with a smart feedback control unit. The system was demonstrated to perform AE detection under low-frequency, large background strain.

The detail design and operation of the smart feedback control scheme is described. The control unit is used to overcome the large quasi-static strains applied on the sensor. The fast speed of the unlocking/relocking process (< 1 ms) assure that the AE signal is monitored without significant disruption. An analysis of the noise that can be coupled to AE signal from electronics resource is provided, and some noise suppression methods has been attempted.

The wavelength tuning characteristics of the laser is studied. First, the wavelength responses to step changes of modulation current were measured for both wavelength “jumping up” and “jumping down”. Different characteristics in terms of the wavelength tuning speed and tuning range were observed for these two cases. Then the wavelength response to sinusoidal current modulation of different frequencies was studied. It is found that the wavelength tuning range decreased as the modulation frequency increased in the frequency range up to 100 kHz.

4.2 Future Work

There are several possibilities for the future investigations to continue improve the smart control unit. There are two improvements can be done on the electronic side. Firstly, reduce the noise that introduced by electronic devices can improve the SNR. As mentioned before, the normalization signal can be directly coupled into the AE signal. More industry level electronic-components can be deployed in the system in the future. Moreover, power supply can also affect the SNR, more stable power supply yields a better result. On the control unit side, 1) we can develop digital P-I controller that is tuned specific for the optical system. 2) More advanced microprocessor can be deployed, and speed up wavelength monitoring

REFERENCE

[1] Thomas Fink, "Ultrasonic Detection Using π -Phase-Shifted Fiber Bragg Gratings",

M.S. Thesis, University of Nebraska, Lincoln, 2012

[2] H. Tsuda, "Ultrasound and damage detection in CFRP using fiber Bragg grating sensors," *Composites science and technology*, vol. 66, pp. 676-683, 2006.

[3] D. C. Betz, *et al.*, "Acousto-ultrasonic sensing using fiber Bragg gratings," *Smart Materials and Structures*, vol. 12, p. 122, 2003.

[4] J. R. Lee, *et al.*, "Impact wave and damage detections using a strain-free fiber Bragg grating ultrasonic receiver," *NDT & E International*, vol. 40, pp. 85-93, 2007.

[5] J. R. Lee, *et al.*, "Single-mode fibre optic Bragg grating sensing on the base of birefringence in surface-mounting and embedding applications," *Optics & Laser Technology*, vol. 39, pp. 157-164, 2007.

[6] Qi Zhang, Yupeng Zhu, Xiangyu Luo, Guigen Liu, and Ming Han, "Acoustic emission sensor system using a chirped fiber-Bragg-grating Fabry–Perot interferometer and smart feedback control" *Opt. Lett.* 42, 631-634 (2017)

[7] L. Hu, G. Liu, Y. Zhu, X. Luo, and M. Han, *IEEE Photonics J.* 8, 1 340 (2016).

- [8] Morthier, P Vankwikelberge, *Handbook of Distributed Feedback Laser Diodes*, Norwiid, MA: ARTECH HOUSE, INC, 1997. pp-10-17
- [9] Xiaowei Dong, Wenkai Liu, Dongyu Wang, Menglong Wu. Study on Fabry–Perot cavity consisting of two chirped fiber Bragg gratings *Optical Fiber Technology* Volume 18, Issue 4, July 2012, Pages 209–214G.
- [10] Raman Kashyap *Fiber Gragg Gratings*, Second Edition, Academy Press, Burlington, MA, 2010.
- [11] Eblana Photonics Technical Staff, *1550nm NLW LASER EP 1550-NLW-B-10*, Eblana Photonics.
- [12] New Focus Technical Staff, *LB1005 High-Speed Servo Controller*, New Focus, P2102297 Rev. A.
- [13] Wikipedia contributors. "PID controller." Wikipedia, The Free Encyclopedia. Wikipedia, The Free Encyclopedia, 27 Mar. 2017. Web. 27 Mar. 2017.
- [14] Arduino AG, "arduinoBoardDue. Arduinio Products," Feb, 2017. [Online]. Available: <https://www.arduino.cc/en/Main/arduinoBoardDue> [Accessed MAR. 01, 2017]

[15] Texas Instrument, “DAC0808 8-Bit D/A Converter”, DAC0808 datasheet, May 1999.

[16] Atmel, “SAM3X / SAM3A Series SMART ARM-based MCU”, SAM3X-SAM3A datasheet, NOV 2009.

[17] A. Sheen, “How to Create +/- Voltage Using One Power Supply,” instructables.com. [Online]. Available: <http://www.instructables.com/id/How-to-create-voltage-using-one-power-supply>. [Accessed Sept. 12, 2016].

[18] Wei-Chih Wang . Seminar. Class Lecture, Topic: “Phase Modulation”
Microtechnology Lab, University of Washington, Seattle, WA.

[19] Lecturer. ELEC 342. Class Lecture, Topic; “Semiconductor Laser Diodes”.
Department of Electrical Engineering, Hong Kong University of Science and
Technology, Clear Water Bay, Hong Kong.

[20] K. O. Hill and G. Meltz, "Fiber Bragg grating technology fundamentals and overview," in *Journal of Lightwave Technology*, vol. 15, no. 8, pp. 1263-1276, Aug 1997.doi: 10.1109/50.618320

[21] Soichi Kobayashi, Yoshihisa Yamamoto, Minoru Ito, and Tatuya Kimura. *Direct Frequency Modulation in AlGaAs Semiconductor Lasers*. IEEE Journal of Quantum Electronics (Volume: 18, Issue: 4, Apr 1982 Pages: 582 – 595)

[22] Tyll Hertsens, *An Overview of Laser Diode Characteristics*, Appl. Note.

[23] Fukuda M, Mishima T, Nakayama N, Masuda T. Temperature and current coefficients of lasing wavelength in tunable diode laser spectroscopy. *Applied physics B, Lasers and optics*. 2010;100(2):377-382. doi:10.1007/s00340-009-3878-0.

[24] S. Kobayashi, Y. Yamamoto, M. Ito and T. Kimura, "Direct frequency modulation in AlGaAs semiconductor lasers," in *IEEE Journal of Quantum Electronics*, vol. 18, no. 4, pp. 582-595, Apr 1982.